A new approach to shallow-depth electromagnetic sounding

Article *in* Russian Geology and Geophysics · May 2017

DOI: 10.1016/j.rgg.2017.04.004

6 authors, including:

E.V. Balkov
A.A. Trofimuk Institute of Petroleum Geology and Geophysics SB RAS
14 PUBLICATIONS **25** CITATIONS
SEE PROFILE

Fadeev Denis
Novosibirsk State University
12 PUBLICATIONS **1** CITATION
SEE PROFILE

Yurii Karin
A.A. Trofimuk Institute of Petroleum Geology and Geophysics SB RAS
11 PUBLICATIONS **22** CITATIONS
SEE PROFILE

G. L. Panin
A.A. Trofimuk Institute of Petroleum Geology and Geophysics SB RAS
10 PUBLICATIONS **21** CITATIONS
SEE PROFILE

Available online at www.sciencedirect.com

ScienceDirect

Russian Geology and Geophysics 58 (2017) 635–641

RUSSIAN GEOLOGY AND GEOPHYSICS

www.elsevier.com/locate/rgg

A new approach to shallow-depth electromagnetic sounding

E.V. Balkov [a,*], D.I. Fadeev [a,b], Yu.G. Karin [a], A.K. Manshtein [a], Yu.A. Manshtein [a,b], G.L. Panin [a]

[a] *A.A. Trofimuk Institute of Petroleum Geology and Geophysics, Siberian Branch of the Russian Academy of Sciences, pr. Akademika Koptyuga 3, Novosibirsk, 630090, Russia*

[b] *Novosibirsk State University, ul. Pirogova 2, Novosibirsk, 630090, Russia*

Received 18 February 2016; accepted 6 July 2016

Abstract

This paper presents an extensive review of currently available shallow-depth portable geophysical instrumentation for electromagnetic induction sounding and profiling and the main technical characteristics of the devices. A new ground-based multicoil shallow-depth device with a special arrangement of receiver coils is considered. The latter are placed on the line where the vertical component of the magnetic field from the source coil is zero. The spacing between the source and the receivers is used as a sounding parameter, along with a frequency. This increases the efficiency of the study of the upper section and the contrast between the sounding curves, which simplifies their interpretation. In studies of local anomalous objects, the use of the proposed method and instrumentation significantly improves the quality of geophysical data. The increase in sounding efficiency provided by these devices is demonstrated on both synthetic and real field data.

Keywords: frequency and geometric sounding; electromagnetic profiling; primary-field compensation

Introduction

Induction sounding and profiling are widely used in shallow geophysics all over the world. The speed and ease of operation of the instrumentation and the quality of the information obtained by these methods determine their applicability for a wide range of problems: from the search of local objects to the identification of structural features of the upper section. The well-known compact sounding devices include GEM-2, EMS, DUALEM, CDM-Explorer (Manshtein et al., 2000; Taylor, 2000; Won et al., 1996). The following electromagnetic profiling instruments are extensively used: EM-31, EM-38, EMP-400, and CMD (McNeill, 1980). The layout of the coils of these instruments is shown in Fig. 1, and their main parameters are listed in Table 1. The effective depth shown in the table is calculated for coplanar coils oriented in the horizontal plane of the coils, as is done, for example, in (Callegary, 2007; McNeill, 1980). The part of the medium above the effective depth provides 70 % of the useful signal. It has also been shown that for the case of coplanar coils oriented in a vertical plane (i.e., orthogonal to the ground), the effective depth is halved. In the case of orthogonally oriented coils in the Dualem instrument (Fig. 1), the effective depth is three times smaller (Taylor, 2000).

The above devices for induction sounding of the subsurface have a number of disadvantages. If the primary field is not compensated, the information content of the useful signal is significantly reduced as it is measured against the background of the primary-field signal with a much larger amplitude. Systems with primary-field compensation are more efficient, but their configuration and calibration require complex electrical circuits and design solutions (Manshtein and Balkov, 2013; Manshtein et al., 2000). Furthermore, in the case of devices in which all coils are located in one plane, one near-surface object may be associated with several images in maps, graphs, and sections, which complicates their interpretation. For example, for the EMS instrument, objects located at a depth of less than 1 m, give rise to several extrema in the signal (Balkov, 2011; Balkov et al., 2013a).

Considerable experience in the development (Balkov et al., 2013b; Manshtein et al., 2000) and application (Epov et al., 2012, 2016) of portable equipment for shallow-depth electromagnetic sounding and profiling has been accumulated at the IPGG SB RAS. Current efforts are directed at developing a new approach to shallow-depth induction sounding in which the source and receiver coils are spaced not only horizontally

* Corresponding author.
E-mail address: BalkovEV@ipgg.sbras.ru (E.V. Balkov)

1068-7971/$ - see front matter © 2017, V.S. Sobolev IGM, Siberian Branch of the RAS. Published by Elsevier B.V. All rights reserved.
http://dx.doi.org/10.1016/j.rgg.2017.04.004

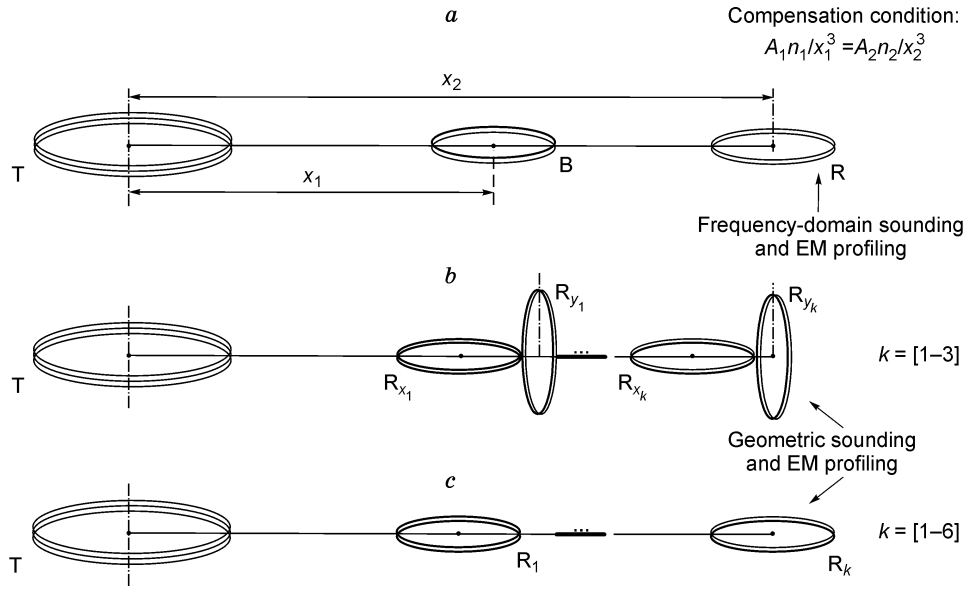

Fig. 1. Different configurations of compact equipment for shallow-depth induction sounding and profiling: *a*, EMS, GEM-2; *b*, Dualem-1, Dualem-21, Dualem-4; *c*, K-1 Em 31-MK2, Em38-MK2-1, EMP-400, CMD; K-2 EM38-MK2; K-3 CMD-EXPLORER; K-6 CMD-MINI-EXPLORER 6L. T is the source coil, B is the compensation coil, and R is the receiver coil.

Table 1. Shallow-depth induction sounding devices and their main characteristics

No.	Type	Device name	Frequency range, kHz	Spacing between the source coil and the receiver coil, m	Effective depth**
1	a	GEM-2	0.03–90	1.68	–
2	a	EMS	2.5–250	1.5*; 2.5	1–5
3	b	Dualem-1	9	1	1.5
4	b	Dualem-2	9	2	4
5	b	Dualem-21	9	1; 2	–
6	b	Dualem-4	9	4	6
7	b	Dualem-42	9	2; 4	6
8	c	EM31-MK2	9.8	3.66	6
9	c	EM31-SH	9.8	2	4
10	c	EM38-MK2-1	14.5	1	0.75
11	c	EM38-MK2	14.5	0.5; 1	0.3; 0.75
12	c	EMP-400	1.0–16	1.21	–
13	c	CMD-Explorer	–	1.48; 2.82; 4.49	2.3; 4.2; 6.7
14	c	CMD-Mini Explorer	–	0.32; 0.71; 1.18	0.5; 1; 1.8
15	c	CMD-Mini Explorer 6L	–	0.2; 0.33; 0.5; 0.72; 1.03; 1.5	0.3; 0.5; 0.8; 1.1; 1.6; 2.3
16	c	CMD Tiny	–	0.45	0.7
17	c	CMD 1	10	0.98	1.5
18	c	CMD 2	10	1.89	3
19	c	CMD 4	10	3.77	6
20	c	CMD 4/6	–	3.77; 5.79	9

Note. Dash indicates the absence of data from the manufacturer.
* Distance between the compensation coil and the source coil.
** Calculated for the horizontal coplanar arrangement of the coils (M_z–H_z mode).

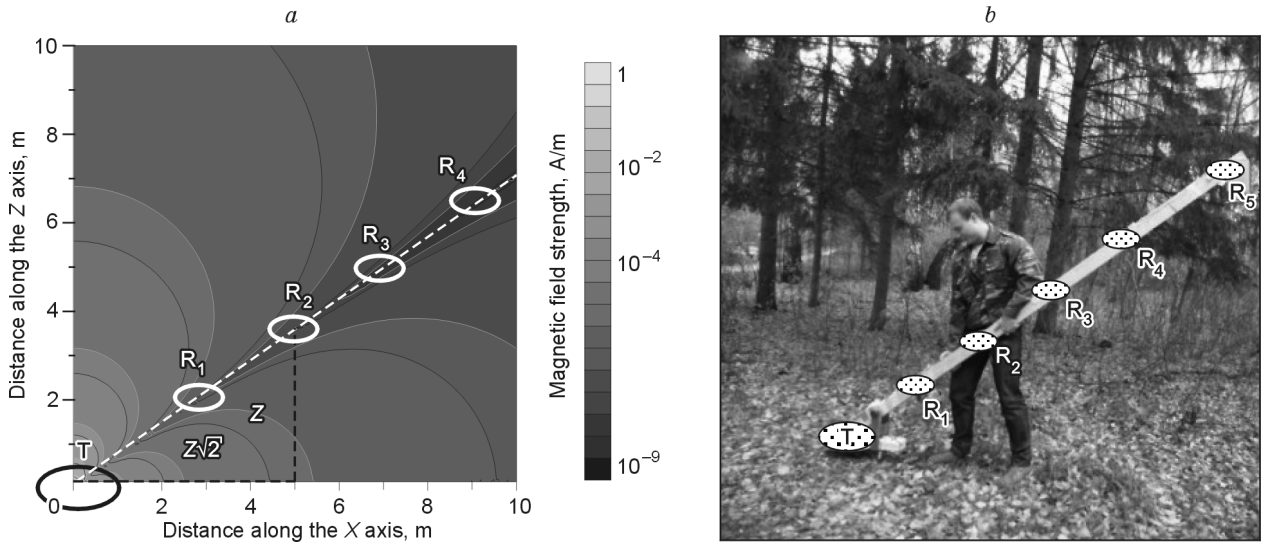

Fig. 2. Signal from a source loop located at the point (0,0) over a half-space with a resistivity of 1000 Ohm·m with the arrangement of coils for the proposed configuration of the radial-frequency sounding (*a*); radial frequency sounding prototype equipment (*b*).

but also vertically. Sounding is performed with a simultaneous change in two parameters: frequency and spacing.

New approach to radial-frequency sounding

In devices such as GEM-2 (developed by the American company Geophex) and EMS (developed by the IPGG SB RAS) (Manshtein et al., 2008), the primary field is compensated using a compensation coil (Won et al., 1996). The compensation diagram and condition are shown in Fig. 1*a*.

Because of the complex configuration process (Manshtein and Balkov, 2013) and problems with false anomalies typical of three-coil devices, the issue of developing an alternative method of primary-field compensation have remained relevant. The magnetic dipole field in an isotropic space has a surface on which the vertical component of the magnetic field vanishes (Fig. 2*a*). The equation of this surface is easily obtained from the expression for the magnetic-dipole field strength in a homogeneous space (Balkov et al., 2006):

$$H_z^t = -\frac{M_t}{4\pi R^3}\left(\frac{3r^2}{R^2} + \frac{3kr^2}{R} + k^2 r^2 - 2 - 2kR\right)e^{-kR}, \quad (1)$$

where $k^2 = i\omega\mu_0\sigma$; r and R are the cylindrical and spherical radii; $M_t = I{\cdot}S{\cdot}n$ is the moment of the source coil, which is the product of the current, area, and the number of turns in the coil; σ is the electrical conductivity of the space. From expression (1) for small kr, we can find the primary-field compensation condition (Yakubovskii, 1980):

$$r \approx \sqrt{2z}. \quad (2)$$

This has made it possible to develop a device in which the set of receiver coils is located in the zone of minimal primary field (Fig. 2*a*) and at different distances from the source. The described method of primary-field compensation and sounding was patented (Balkov et al., 2013b). In this case, the variable parameters used to increase the sounding capability are the frequency and the distance between the source and the receiver.

Mathematical apparatus for modeling

The vertical component of the magnetic field strength of a vertical magnetic dipole located on the surface of a nonmagnetic horizontally layered medium is calculated from the expression

$$H_z = \frac{M_t}{2\pi}\int_0^\infty \lambda^3 J_0(\lambda r)\, X_N\, d\lambda, \quad (3)$$

where N is the number of layers, X_N is a layered function which is calculated using a recursive algorithm (Balkov et al., 2006; Mogilatov, 1993).

The layered functions of a homogeneous half-space (X_1) and a two-layer medium (X_2) are given by

$$X_1 = -\frac{1}{(p_0 + p_1)}\, e^{-p_1 z}, \quad (4)$$

$$X_2 = -\frac{p_1{\cdot}\mathrm{ch}(p_1{\cdot}h) + p_2{\cdot}\mathrm{sh}(p_1{\cdot}h)}{(p_0{\cdot}p_1 + p_1{\cdot}p_2){\cdot}\mathrm{ch}(p_1{\cdot}h) + (p_1^2 + p_0{\cdot}p_2){\cdot}\mathrm{sh}(p_1{\cdot}h)}\, e^{-p_1 z}, \quad (5)$$

where $p_j^2 = \lambda^2 + k_j^2$, $k_j^2 = i\omega\mu_0\sigma_j$, $j = 0, \ldots, 2$, $z \geq 0$.

The emf (ε_d) and the current (I_d) in the receiver coil approximated by the dipole can be found from the formulas

$$\varepsilon_d = i\omega\mu_0 M_d H_z(r_d, z_d),\ I_d = \varepsilon_d / Z_d, \quad (6)$$

where M_d, r_d, z_d, and Z_d are the moment, horizontal and vertical positions, and impedance of the receiver coil.

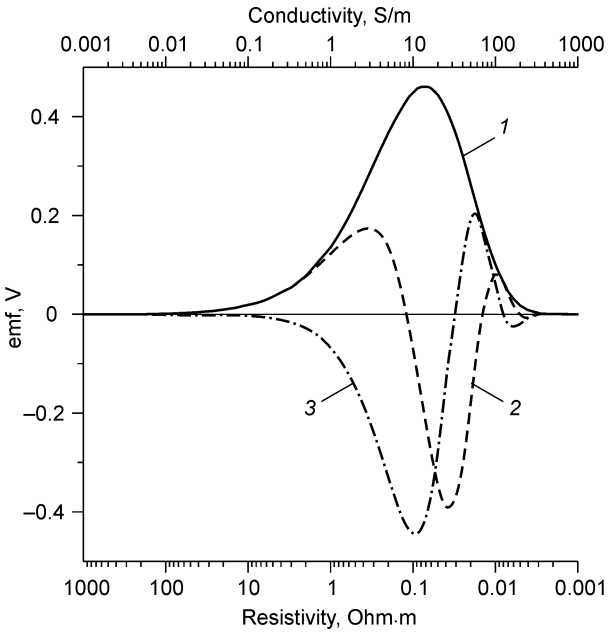

Fig. 3. Measured emf (for different components) in the receiver coil versus resistivity of the medium: *1*, module, *2,* quadrature, *3,* in-phase.

Data transformation

Figure 3 shows curves of the various components of the integrated emf (quadrature, in-phase, and module) calculated according to formulas (3), (4), and (6) as functions of the electrical conductivity of a homogeneous half-space for a frequency of 250 kHz and a horizontal spacing (r) of 0.5 m. The process of determining the electrical conductivity from measured emf values in this model is called signal transformation that gives apparent electrical conductivity values. This is done by solving the corresponding transcendental equation. These functions are not unique throughout the range of electrical conductivity of the half-space. Therefore, to correctly determine the apparent values, the solution is performed in the regions of monotonicity of the measured emf as a function of the resistivity of the medium (Fadeev and Balkov, 2014). The results of transformations of synthetic signals calculated for two- and three-layer models will be demonstrated below.

Data modeling and transformation for layered media

The applicability of the proposed device can be shown based on the transformation of model data. A wide range of horizontally layered models was studied. The simplest is a two-layer geoelectric section.

Figure 4 shows a comparison of curves of the apparent resistivity, frequency (EMS instrument) and radial-frequency sounding (RFS). The calculations were performed for 14 fixed frequencies of the EMS instrument. In Fig. 4*a*, the electrical resistivity of the overlying layer is 100 Ohm·m and that of the underlying layer is 10 Ohm·m; in Fig. 4*b*, the situation is reverse.

As can be seen, the apparent resistivity curves for the radial-frequency sounding device are more pronounced than

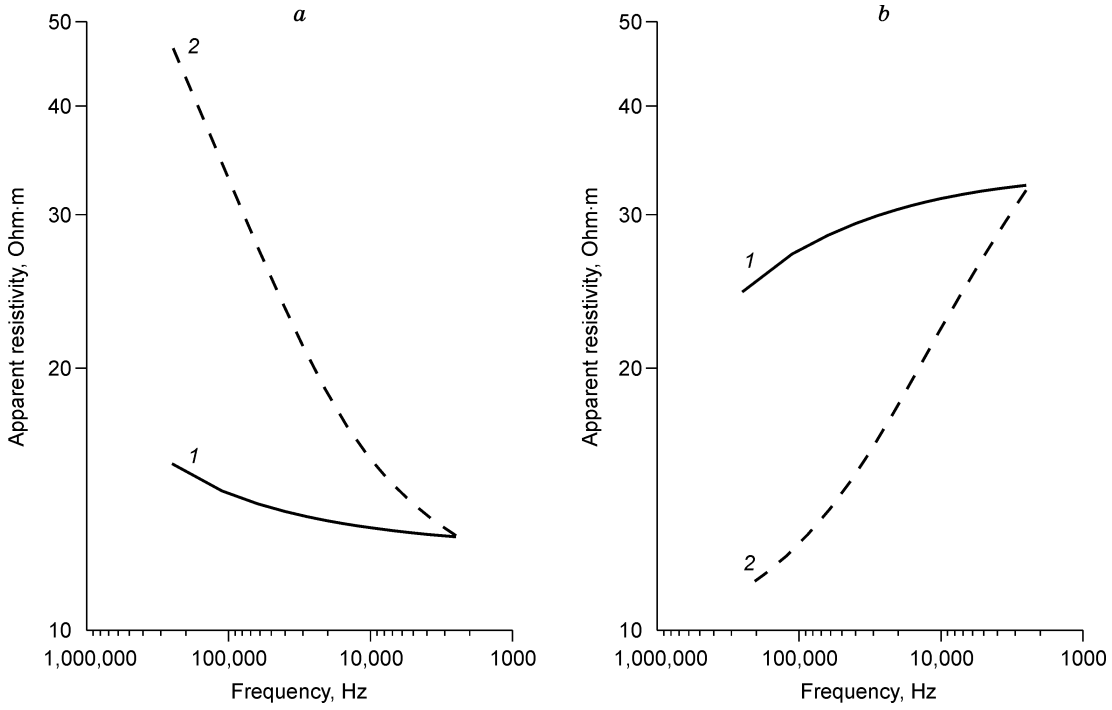

Fig. 4. Comparison of sounding curves for the EMS (*1*) and radial-frequency sounding (RFS) (*2*) equipment. *a*, Two-layer model: the upper-layer has a resistivity of 100 Ohm·m and thickness of 1 m, and the underlying layer has a resistivity of 10 Ohm·m; *b*, two-layer model: the upper layer has a resistivity of 10 Ohm·m and thickness of 1 m, and the underlying layer has a resistivity of 100 Ohm·m.

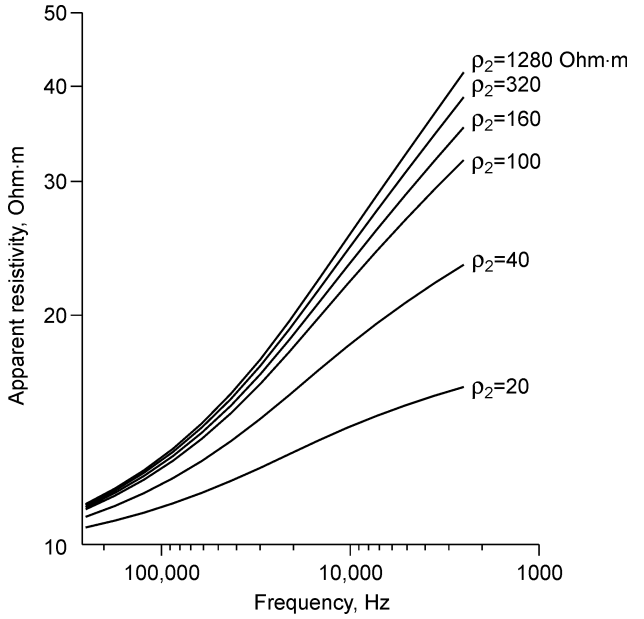

Fig. 5. Calculated RFS sounding curves for a two-layer earth model: the first layer has a resistivity of 10 Ohm·m and thickness of 1 m, and the resistivity of the second infinite layer varies from 20 to 1280 Ohm·m.

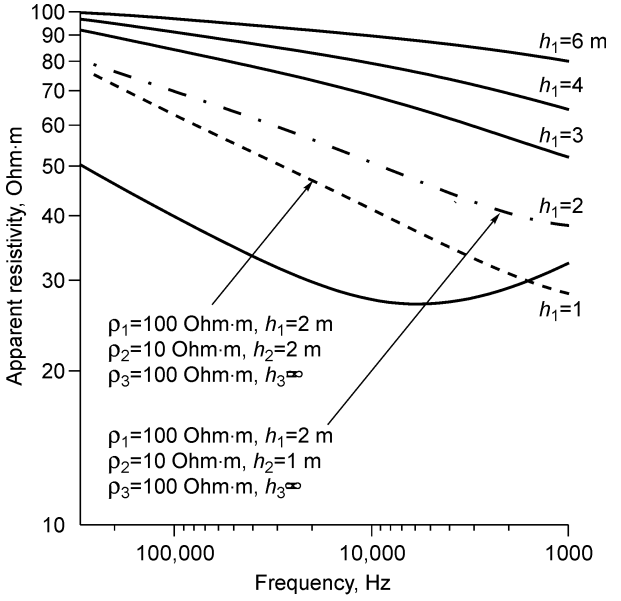

Fig. 6. Theoretical sounding curves for three-layer models in which the more conductive layer (ρ_1 = 10 Ohm·m, h_1 = 1 m) is buried to various depths (indicated in the graphs) into the less conductive layer (resistivity of 100 Ohm·m). The dashed curve was calculated for the model with the conductive-layer thickness increased to 2 m.

those for the EMS device, suggesting good prospects for the use of this sounding configuration.

Further calculations were performed for a two-layer medium in which the first layer has an electrical resistivity of 10 Ohm·m and a thickness of 1 m and the electrical resistivity of the underlying space ranges from 20 to 1280 Ohm·m (Fig. 5). In this case, the apparent resistivity curves are distinct and easy to interpret. The left asymptote for all the graphs is the resistivity of the upper conductive layer. The level of the right asymptote changes depending on the resistivity contrast between the layers. It can be seen that up to a resistivity ratio equal to 32 (the first layer has a resistivity of 10 Ohm·m, and the second layer a resistivity of 320 Ohm·m), the curves differ considerably from each other and can be separated even at a qualitative level. Further, the graphs for the model with a second-layer resistivity of 320 and 1280 Ohm·m differ at a frequency of 2.5 kHz by only 7.5% (maximum difference), which is close to the measurement error of the device of 5%. This leads to a limitation on the exploration of sections with a resistivity of more than 300 Ohm·m.

The search for highly conductive thin horizons overlain by a layer of high-resistivity rocks (three-layer sections of type H) is an important task. It is first appropriate to investigate the behavior of the sensitivity of the radial-frequency sounding device on the surface of a three-layer medium where the resistivities of the first and last layers are high and a conductive layer with resistivity ρ_2 and thickness h_2 lies at depth h_1.

Figure 6 shows calculated apparent resistivity curves for a medium with the geoelectric section described above. The calculations were performed for a conductive layer buried to different depths of 1 to 6 m from its roof. As can be noted, the sensitivity to the conductive layer is retained up to a depth of 6 m. However, the possibility of determining the parameters of the conductive layer is significantly reduced when the thickness of the first layer is greater than 2 m. It is worth noting that the effect of the less conductive underlying layer is apparent to a depth of 2 m.

It is of interest to estimate the thickness of the conductive layer. Increasing it to a level of 2 m (see Fig. 6), we see a significant reduction in the apparent resistivity at low frequencies. Both the slope of the graph and its behavior at around 1.5 kHz changed. At a lower thickness of the conductive horizon, the response of the underlying layer is still felt, which can be a characteristic criterion for estimating the parameters of the conductor.

Modeling of local inhomogeneity

Another important application of induction instrumentation is the search for local objects with anomalous electrical resistivity. Examples of such objects are archaeological sites, waste disposals, unexploded ordnance, etc. The results of modeling this problem with the coils and the local conductor approximated by vertical magnetic dipoles in a poorly conductive homogeneous medium are given below.

The alternating magnetic field of the source induces an emf in a local conductive object, which can be calculated by formulas (1) and (6). Then, the current induced in this object is calculated by the same formulas and is used as the source to calculate the useful emf in the receiver coil.

The calculation results are given in Fig. 7 for three different types of devices: *a*, type c, and a radial-frequency device

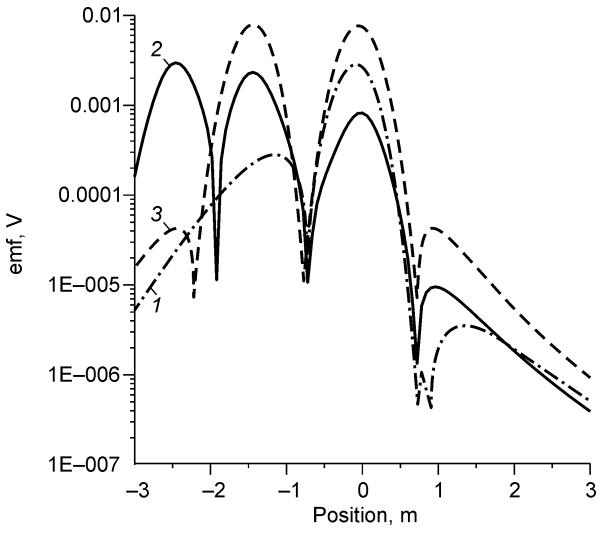

Fig. 7. Synthetic signal over a local conductive object located at a depth of 0.5 m (position 0 m) obtained at a frequency of 50 kHz for RFS (*1*) and EMS (*2*) devices and C type equipment (*3*).

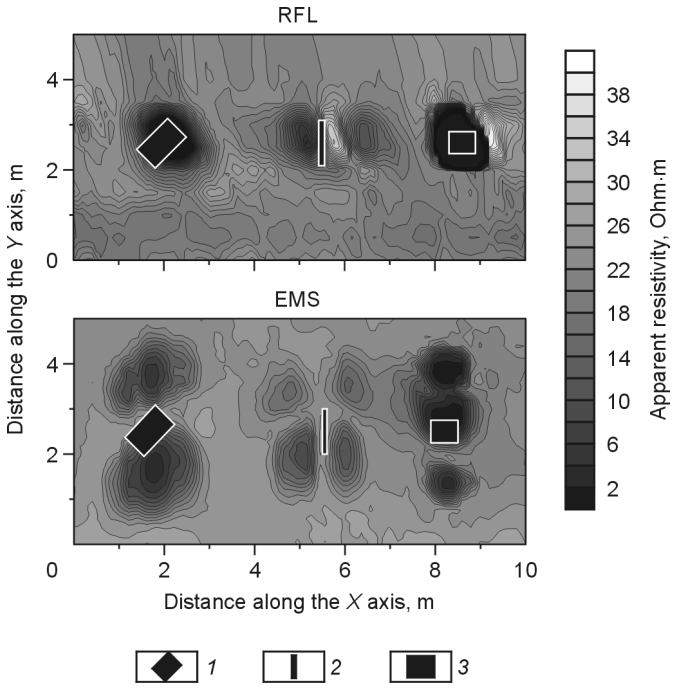

Fig. 8. Apparent resistivity distribution maps obtained using the EMS equipment and radial-frequency sounding over three local conductive objects. *1*, horizontal copper sheet (10 × 0.6 m), depth 0.8 m; *2,* vertical copper sheet (10 × 0.6 m), depth to the top 0.45 m; *3,* horizontal copper sheet (0.5 × 0.6 m), depth 0.2 m.

(Table 1). The figure also shows the modulus of the complex signal amplitude versus the position of the device along the profile which passes over a local conductor buried to a depth of 0.5 m (simulated by a magnetic dipole with moment equivalent to a single-turn copper loop with a radius of 0.2 m).

In the profile diagrams, three extrema are observed for the three-coil device (type a, Table 1), two distinct extrema for the two-coil device (types b and c), and one dominant extremum at the center of the source coil for the RFS device. The results of similar calculations for different depths of the conductive object and different spacings and frequencies are given in (Balkov, 2011a). Another finding is that one extremum in the signal begins to dominate with increasing depth of the point conductor. This occurs when the depth of the object is comparable to or exceeds the spacing between the coils. For the RFS equipment with any spacings and depths of the object, one extremum dominates.

The modeling results demonstrate the advantage of the new RFS device and the difficulties with which the interpreter will have to face in the presence of several near-surface objects when using commercial equipment (Table 1, types a, b, and c).

Prototype equipment, example of field data, and prospects of development

To confirm the results based on synthetic data, we conducted field tests of the RFS prototype equipment and EMS equipment at the geoelectric test site of the IPGG SB RAS (Balkov et al., 2013a). The RFS prototype equipment comprised one source coil (from the EMS equipment) and five coils (Fig. 2*b*), each of which could be used for measurements at 14 frequencies (Table 1). The horizontal spacing was in the range from 0.5 to 2.5 m to provide that $r \approx \sqrt{2z}$. When operating the equipment, it is important that the permanent the systems of the equipment be at a constant distance from the ground. An error of 10 cm in the position of the device leads, on average, to a change of no more than 10% in the signal, which is acceptable.

Figure 8 shows the results of areal profiling at a frequency of 28 kHz. The survey was carried out with a constant orientation of the device. Three metal targets with different spatial orientations were laid at different depths in the study area (Fig. 8). All the targets were at a depth of not more than 1 m, so that they were responsible for several extrema in the signal. For the three-coil EMS equipment, horizontally oriented targets produce two or three images, which is consistent with the results of mathematical modeling (Balkov, 2011b). Vertically oriented targets produce more complex anomalies similar in shape to quadrupoles. In studies using the RFS prototype equipment, horizontally oriented objects are manifested in a single (for an object at a depth of 0.8 m) or one dominant anomaly (object at a depth of 0.2 m). A vertically oriented object is manifests by several anomalies, as in the case of EMS. The field tests generally confirm the conclusions drawn from the result of mathematical modeling.

Analysis of a large number of experimental data obtained using the described prototype equipment over more than a dozen objects at the test site (Khalatov and Balkov, 2014) suggests two promising lines of development of the prototype equipment. Since most local conductive objects laid at a depth of 3 m can be detected by a short device (horizontal spacing of 0.5 m) at one of two frequencies close to 10 and 100 kHz, it is promising for profiling purposes to develop compact

two-frequency two-coil equipment. For sounding, it is necessary to develop multicoil RFS equipment, whose prototype is shown in Fig. 2*b*.

Conclusions

The proposed arrangement of coils along a straight line at an angle to the plane of the source provides primary-field compensation, which allows the quadrature and in-phase signal components to be measured in pure form. This improves the noise immunity because the measurement of small useful signals against the background of large primary-field amplitudes is avoided. In addition, measurements of the in-phase component provide additional information for signal interpretation (Huang and Fraser, 2001).

Theoretical and practical explorations show that anomalous local objects produce a too complex signal for the currently used compact electromagnetic devices. The signal contains one to four extrema from one anomalous object. The proposed new configuration of the receiver coils provides a single dominant anomaly of the signal over an object.

The proposed radial-frequency sounding configuration provides a simultaneous change in frequency and spacing, which increases the sounding efficiency compared with sounding for one parameter. The mathematical modeling shows that this equipment configuration is promising for studying the properties of the upper part (up to 10 m) of geoelectric sections. The maximum efficiency and contrast of apparent resistivity curves are observed in studies of media with a resistivity of 300 Ohm·m.

It is planned to implement the above principles and prototype equipment in production versions and test them in solving practical problems.

References

Balkov, E.V., 2011a. Technology of shallow-depth frequency sounding. Geofizika, No. 6, 42–47.

Balkov, E.V., 2011b. Multiple images in signals from local objects in electromagnetic profiling using a compact device with spaced coils, in: All-Russian M.N. Berdichevsky and L.L. Van'yan Workshop on Electromagnetic Sounding of the Earth. May 16–21, 2011. St. Petersburg, p. 4.

Balkov, E.V., Epov, M.I., Manshtein, A.K., 2006. Evaluation of the depth of electromagnetic induction frequency ground-based sounding. Geofizika, No. 3, 41–44.

Balkov, E.V., Stoikin, T.A., Manshtein, A.K., Karin, Yu.G., 2013a. The results of shallow frequency-domain ground-based sounding at the geoelectric test site of the Institute of Petroleum Geology and Geophysics SB RAS (Novosibirsk). Geofizicheskie Issledovaniya 14 (3), 55–63.

Balkov, E.V., Manshtein, A.K., Sukhorukova, K.V., Epov, M.I., 2013b. A method for calibrating a device for electromagnetic induction frequency ground sounding. RF Patent No. 2461850, MPK8 G01V13/00, 28.06.2010, Byul. No. 26.

Callegary, J.B., Ferre, P.A., Groom, R.W., 2007. Vertical spatial sensitivity and exploration depth of low-induction-number electromagnetic-induction instruments. Vadose Zone J. 6, 158–167.

Epov, M.I., Balkov, E.V., Chemyakina, M.A., Manshtein, A.K., Manshtein, Yu.A., Napreev, D.V., Kovbasov, K.V., 2012. Frozen mounds in Gorny Altai: geophysical and geochemical studies. Russian Geology and Geophysics (Geologiya i Geofizika) 53 (6), 583–593 (761–774).

Epov, M.I., Molodin, V.I., Manshtein, A.K., Balkov, E.V., Dyad'kov, P.G., Matasova, G.G., Kazanskii, A.Yu., Bortnikov, S.B., Pozdnyakova, O.A., Karin, Yu.G., Kuleshov, D.A., 2016. Integrated archeological and geophysical studies in West Siberia. Russian Geology and Geophysics (Geologiya i Geofizika), 57 (3), 473–482 (603–614).

Fadeev, D.I., Balkov, E.V., 2014. Algorithmic maintenance and testing sounding the possibilities of equipment radial frequency sounding, in: Near Surface Geoscience 2014: Proc. 20th European Meeting of Environmental and Engineering Geophysics. Athens, Greece. Curran Associates, Inc., Red Hook, pp. 645–649.

Huang, H., Fraser, D.C., 2001. Mapping of the resistivity, susceptibility, and permittivity of the earth using a helicopter-borne electromagnetic system. Geophysics 66 (1), 148–157.

Khalatov, S.Yu., Balkov, E.V., 2014. Equipment of radial-frequency sounding and electromagnetic profiling, in: Proc. 27th Annual Symposium on the Application of Geophysics to Engineering and Environmental Problems. Boston, USA, p. 147.

Manshtein, A.K., Balkov, E.V., 2013. A method and device for frequency-domain induction sounding. RF Patent No. 2502092, MPK8 G01V3/10, 01.08.2011. Byul. No. 25.

Manshtein, A.K., Epov, M.I., Voevoda, V.V., Sukhorukova, K.V., 2000. A method of induction frequency sounding. RF Patent No. 2152058, MPK7 G01V3/10, 24.06.1998. Byul. No. 18.

Manshtein, A.K., Panin, G.L., Tikunov, S.Yu., 2008. A device for shallow frequency-domain electromagnetic induction sounding, Russian Geology and Geophysics (Geologiya i Geofizika) 49 (6), 430–436 (571–579).

Mogilatov, V.S., 1993. A way of solving fundamental direct problems of TES. Geologiya i Geofizika (Russian Geology and Geophysics) 34 (3), 108–117 (104–113).

McNeill, J.D., 1980. Electromagnetic terrain conductivity measurement at low induction numbers. Tech. Note TN-6. Geonics Ltd., Mississauga, Ontario.

Taylor, R.S., 2000. Mapping sites of environmental contamination with a dual-geometry electromagnetic (EM) system, in: Proceeding of the Society of Exploration Geophysicists Annual Meeting, Expanded Abstracts, E12.

Won, I.J., Keiswetter, D.A., Fields, G.R.A., Sutton, L.C., 1996. GEM-2: A new multifrequency electromagnetic sensor. J. Environ. Eng. Geophys. 2 (1), 129–138.

Yakubovskii Yu.V., 1980. Geoelectrics [in Russian]. Nedra, Moscow.

Editorial responsibility: M.I. Epov